

## MHD Flow and Nonlinear Thermal Radiative Heat Transfer of Dusty Prandtl Fluid over a Stretching Sheet

K. Ganesh Kumar<sup>1,\*</sup>, S. Manjunatha<sup>2</sup> and N. G. Rudraswamy<sup>3</sup>

**Abstract:** Boundary layer flows and melting heat transfer of a Prandtl fluid over a stretching surface in the presence of fluid particle suspensions has been investigated. The converted set of boundary layer equations are solved numerically by RKF-45 method. Obtained numerical results for flow and heat transfer characteristics are deliberated for various physical parameters. Furthermore, the skin friction coefficient and Nusselt number are also presented in Tabs. 2 and 3. It is found that the heat transfer rates are advanced in occurrence of nonlinear radiation compared to linear radiation. Also, it is noticed that velocity and temperature profile increases by increasing Prandtl parameter.

**Keywords:** Prandtl fluid, melting effect, dusty fluid, nonlinear radiation.

### Nomenclature

$B_0^2$	magnetic field	$q_w$	heat flux at the surface
$b$	stretching rate	$q_r$	radiative heat flux ( $Wm^{-2}$ )
$c_p$	fluid phase specific heat coefficient ( $J/kgK$ )	$R$	radiation parameter
$c_m$	dust phase specific heat coefficient ( $J/kgK$ )	$r$	radius of dust particles
$C_f$	skin friction coefficient	$Re_x$	local Reynolds number
$Ec$	Eckert number	$Sh_x$	Sherwood number
$f$	dimensionless velocity of the fluid phase	$T$	temperature of the fluid phase ( $K$ )
$F$	dimensionless velocity of the dust phase	$T_p$	temperature of the dust phase ( $K$ )
$K$	Stokes drag constant	$T_m$	temperature of the melting surface ( $K$ )
$k$	thermal conductivity ( $W/m K$ )	$T_\infty$	ambient fluid temperature ( $K$ )
$k^*$	mean absorption coefficient ( $W/m K$ )	$u_w$	stretching sheet velocity ( $m s^{-1}$ )
$l$	mass concentration of dust particles parameter	$u, u_r$	velocity components of fluid phase ( $m s^{-1}$ )

<sup>1</sup> Department of Mathematics, SJM Institute of Technology, Chitradurga, 577502, India.

<sup>2</sup> Department of Engineering Mathematics, Faculty of Engineering, Christ University, Bengaluru, 560074, India.

<sup>3</sup> Department of Studies and Research in Mathematics, Kuvempu University, Shimoga, 577451, India.

\* Corresponding Author: K. Ganesh Kumar. Email: ganikganesh@gmail.com.

Received: 28 January 2018; Accepted: 20 February 2019.

$M$	magnetic parameter	$v, v_p$	velocity components of dust phase ( $m s^{-1}$ )
$m^*$	mass of dust particles		
$m$	dimensionless melting parameter	$A$ and $c$	material constants
$N$	dust particles number density	$x$	coordinate along the plate ( $m$ )
$Nu_x$	local Nusselt number	$y$	coordinate normal to the plate ( $m$ )
$Pr$	Prandtl number	$\frac{c_f(T_\infty - T_m)}{\lambda}$	Stefan number for the liquid phase
$\frac{c_s(T_m - T_\infty)}{\lambda}$	Stefan number for the solid phases		

### Greek symbols

$\beta_v$	fluid-particle interaction parameter for velocity	$\tau_w$	surface shear stress
		$\tau_v$	dust particles relaxation time
$\alpha$	Prandtl parameter	$\beta$	elastic parameter
$\beta_t$	fluid-particle interaction parameter	$\gamma$	specific heat ratio
$\mu$	temperature dynamic viscosity ( $kg m^{-1}s^{-1}$ )	$\rho$	base fluid density ( $kg/m^3$ )
$\nu$	kinematic viscosity ( $m^2s^{-1}$ )	$\rho_p$	dust particles density ( $kg/m^3$ )
$\sigma$	electrical conductivity of the fluid	$\Gamma$	the time constant
$\sigma^*$	Stefan-Boltzmann constant ( $W m^{-2}K^{-4}$ )		<b>Superscript:</b>
$\theta$	dimensional fluid phase temperature	'	derivative with respect to $\eta$
$\theta_p$	dimensional dust phase temperature		<b>Subscript:</b>
$\eta$	similarity variable	$p$	particle phase
$\tau_T$	thermal equilibrium time	$\infty$	fluid properties at ambient condition.

## 1 Introduction

Suspended particles in a clean fluid represented by a mathematical two-phase model find numerous technological applications during the electrostatic precipitation, fluidization, combustion, centrifugal separation of matter from fluid, nuclear processing, polymer technology, physiological flows, purification of crude oil, nuclear reactor cooling, performance of solid fuel rocket nozzles and paint spraying etc. Saffman [Saffman (1962)] analyzed the flow of a dusty gas in which the fluid suspension particles are uniformly distributed. Further, Siddiqa et al. [Siddiqa, Hossain and Saha (2015)] analyzed the natural convection flow of a dusty fluid, and they have interpreted for wide range of Prandtl number: it is observed that thin boundary layer structures can be formed when there is an effect of mass concentration parameter or Prandtl number. Prakash et al. [Prakash, Makinde, Kumar et al. (2015)] studied the heat transfer to MHD oscillatory dusty fluid flow in a channel filled with a porous medium, and they conclude that the dusty fluid temperature enhances while the Nusselt number minimizes with increasing values of radiation parameter. Mustafa [Mustafa (2017)] investigated the two-phase dusty fluid flow and heat model over deforming isothermal surfaces. Isa et al. [Isa and Mohammad (2017)] discussed the boundary layer flow of dusty fluid on a stretching sheet of another quiescent fluid and found that an uplifting value of fluid particle interaction parameter contributes to

enhance the velocity of dust phase, but scale back the velocity of fluid phase. A number of analysis to the heat transfer over a suspended particle under different physical conditions were intensely made in recent years [Krishnamurthy, Kumar, Gireesha et al. (2018); Reddy, Rani, Kumar et al. (2018); Kumar, Manjunatha, Gireesha et al. (2017); Kumar, Rudraswamy, Gireesha et al. (2017); Kumar, Gireesha and Gorla (2018)].

Now a days, the studies of fluid flow through a melting heat transfer are extensively indulged among mathematicians, engineers, physicians, scientists and medical practitioners. There are many diverse applications including the casting, welding and magma solidification, permafrost melting and softening of frozen ground etc. Bachok et al. [Bachok, Ishak and Pop (2010)] discussed the steady two-dimensional stagnation-point flow and heat transfer of a melting stretching/shrinking sheet. Makinde et al. [Makinde, Kumar, Manjunatha et al. (2017)] discussed an effect of nonlinear thermal radiation on MHD boundary layer flow and melting heat transfer of micro-polar fluid over a stretching surface. Mabood et al. [Mabood, Shafiq, Hayat et al. (2017)] presented the radiation effects on stagnation point flow with melting heat transfer and second order slip, and they concluded that the temperature profile decreases for larger values of melting parameter, and it has quite opposite behavior for concentration profile. Kumar et al. [Kumar, Gireesha, Prasannakumara et al. (2017)] initiated the phenomenon of radiation and viscous dissipation on Casson nanoliquid flow past a moving melting surface. Gireesha et al. [Gireesha, Kumar, Rudraswamy et al. (2017)] studied the melting heat transfer of hyperbolic tangent fluid over a stretching sheet with fluid particle suspension and thermal radiation. Arici et al. [Arici, Ensar, Kan et al. (2017)] discussed the melting of nanoparticle-enhanced paraffin wax in a rectangular enclosure with partially active walls. Mohsen et al. [Mohsen and Sadoughi (2018)] analyzed the simulation of  $CuO$ -water nanofluid heat transfer enhancement in presence of melting surface.

The linearized form of the Rosseland approximation is valid only when the temperature difference between the solid boundary and the ambient fluid is low. But, nonlinear Rosseland radiation approximation is valid for low and high temperature difference between the wall and the bulk fluid. Furthermore, the temperature profile is S-shaped in a case of nonlinear Rosseland approximation as compared to a linear approximation. In view of this advantage, various researcher published papers about heat transfer over a nonlinear thermal radiation. Makinde et al. [Makinde and Animasaun (2016)] discussed the thermophoresis and Brownian motion effects on MHD bioconvection of nanofluid with nonlinear thermal radiation and quartic chemical reaction past an upper horizontal surface of a paraboloid of revolution. Hayat et al. [Hayat, Qayyum, Imtiaz et al. (2016)] presented the comparative study of silver and copper/water nanofluids with mixed convection and nonlinear thermal radiation. Afridi et al. [Afridi and Qasim (2018)] investigated the entropy generation and heat transfer in boundary layer flow over a thin needle moving in a parallel stream in the presence of nonlinear Rosseland radiation. Kumar et al. [Kumar, Archana, Gireesha et al. (2018)] discussed the cross diffusion effect on MHD mixed convection flow of nonlinear radiative heat and mass transfer of Casson fluid over a vertical plate. Gireesha et al. [Gireesha, Ramesh, Kumar et al. (2018)] studied the nonlinear convective heat and mass transfer of Oldroyd-B nanofluid over a stretching sheet in the presence of uniform heat source/sink.

The study of non-Newtonian fluids is one of the thrust areas of contemporary research because of their colossal potential regarding improved heat transfer. For example, food mixing, flow of blood, plasma, mercury amalgams and lubrications with heavy oils and greases. In view of these applications, many studies are focused on non-Newtonian fluids. Akbar et al. [Akbar, Nadeem, Haq et al. (2013)] discuss the Numerical solutions of Magneto hydrodynamic boundary layer flow of tangent hyperbolic fluid flow towards a stretching sheet with magnetic field. Nasrin et al. [Nasrin and Alim (2012)] analyzed the Prandtl number effect on free convective flow in a solar collector utilizing nanofluid. Nadeem et al. [Nadeem, Ijaz and Akbar (2013)] studied the nanoparticle analysis for blood flow of Prandtl fluid model with stenosis. Rehena et al. [Rehena, Salma and Alim (2016)] initiated the Prandtl number effect on assisted convective heat transfer through a solar collector. A few recent attempts in this direction can be stated through studies, Mishra et al. [Mishra, Khan, Al-mdallal et al. (2015); Shamsuddin, Beg, Ram et al. (2017); Khan, Malik, Hussain et al. (2017); Hussain, Malik, Awais et al. (2017); Malik, Hussain, Salahuddin et al. (2016); Beg, Thumma and Kadir (2017); Thumma and Shamsuddin (2018)].

In view of the above the investigations, it is worth noticing that little attention has been given to investigate the motion of melting heat transfer and nonlinear thermal radiation effect on flow and heat transfer of Non Newtonian fluids. In the present study, we intend to analyze the boundary layer flow and melting heat transfer of a Prandtl fluid over a stretching surface in the presence of fluid particles suspension. The governing systems of partial differential equations have been transformed to a set of coupled ordinary differential equations by applying appropriate similarity transformations. The reduced equations are solved numerically. The pertinent parameters are discussed through tables and plotted graphs.

## 2 Mathematical formulation

Steady flow of an incompressible Prandtl fluid with suspended dust particles over a stretching sheet is considered. The flow is assumed to be confined to a region of  $y > 0$ . The flow is generated by action of two equal and opposite forces along the  $x$ -axis and  $y$ -axis being normal to the flow. A uniform magnetic field  $B_0$  is imposed along  $y$ -axis, and sheet is being stretched with velocity  $u_w(x)$  along  $x$ -axis. Let  $T_m$  be the temperature of the melting surface while the temperature in the free-stream condition is  $T_\infty$ , where  $T_\infty > T_m$ .

The governing equations of motion of dusty fluid with uniform distribution of fluid and dust particles are:

**For fluid phase:**

$$\frac{\partial \rho}{\partial t} + \nabla \cdot (\rho \vec{u}) = 0, \quad (2a)$$

$$\rho((\vec{u} \cdot \nabla) \vec{u}) = \nu \frac{A}{c} \nabla^2 \vec{u} + \frac{\nu A}{2c^3} (\nabla u)^2 + KN(\vec{v} - \vec{u}) + \sigma B_0^2 \nabla \vec{u}, \quad (2b)$$

$$\rho C_p((\vec{u} \cdot \nabla) E) = Q + (\vec{v} - \vec{u}) \cdot \vec{F} + k \nabla \cdot (\nabla T) - \nabla q_r, \quad (2c)$$

**For dust phase:**

$$\nabla \cdot (N \vec{v}) = 0 \quad (2d)$$

$$\rho_p((\vec{v} \cdot \nabla) \vec{v}) = \vec{g} + KN(\vec{u} - \vec{v}) \quad (2e)$$

where  $\vec{u}$  and  $\vec{v}$  are the velocity for the fluid and dust phase respectively,  $Q = \frac{\rho_p c_p (T_p - T)}{\tau T}$  is the thermal interaction between fluid and dust particles phase,  $F = \frac{(\vec{v} - \vec{u})}{\tau_v}$  is the velocity of interaction force between the fluid and dust,  $\tau_v = \frac{m}{6\pi a \mu} = \frac{m}{K}$  is the velocity relaxation time of dust particles,  $\tau_v = \frac{m c_p}{4\pi a k}$  is the thermal relaxation time of the dust particles,  $k \nabla \cdot (\nabla T)$  is the rate of heat added to the fluid by conduction in unit volume.  $\rho, p, \nu, T, C_p$  and  $k$  are density, pressure, kinematic viscosity, temperature, specific heat and thermal conductivity of the fluid respectively.  $\rho_p = mN$  is density of dust particle.  $N, T_p, c_m$  and  $m$  are number density, temperature, specific heat and mass concentration respectively.

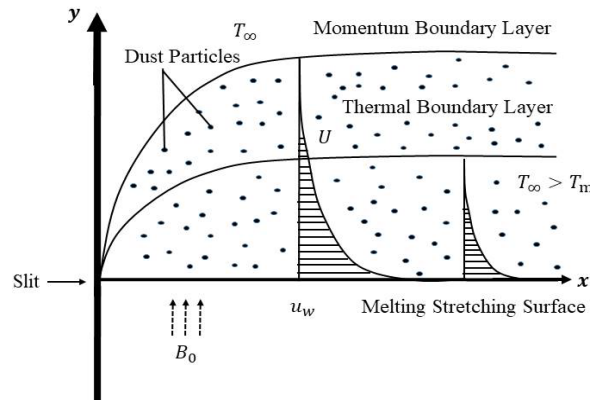


**Figure 1:** Flow configuration and coordinate system

Under the boundary layer approximations, the governing Eqs. 2(a), 2(b), 2(d) and 2(e) take the following forms,

$$\frac{\partial u}{\partial x} + \frac{\partial v}{\partial y} = 0, \tag{2.1}$$

$$u \frac{\partial u}{\partial x} + v \frac{\partial u}{\partial y} = \nu \frac{A}{c} \frac{\partial^2 u}{\partial y^2} + \frac{\nu A}{2c^3} \left( \frac{\partial u}{\partial y} \right)^2 \frac{\partial^2 u}{\partial y^2} + \frac{KN}{\rho} (u_p - u) - \frac{\sigma B_0^2}{\rho} u, \tag{2.2}$$

$$\frac{\partial u_p}{\partial x} + \frac{\partial v_p}{\partial y} = 0, \tag{2.3}$$

$$\rho_p \left( u_p \frac{\partial u_p}{\partial x} + v_p \frac{\partial u_p}{\partial y} \right) = KN (u - u_p), \tag{2.4}$$

The appropriate boundary conditions applicable to the present problem are:

$$\begin{aligned} u &= u_w, \text{ at } y = 0, \\ u &\rightarrow 0, \quad u_p \rightarrow 0, \quad v_p \rightarrow v \text{ as } y \rightarrow \infty, \end{aligned} \tag{2.5}$$

Eqs. (2.1)-(2.4) subjected to boundary conditions Eq. (2.5) admits self-similar solution in terms of the similarity functions  $f, F$  and similarity variable  $\eta$ , and they are defined as:

$$\begin{aligned} u &= bx f'(\eta), \quad v = -\sqrt{vb} f(\eta), \quad \eta = \sqrt{\frac{b}{\nu}} y, \\ u_p &= bx F'(\eta), \quad v_p = -\sqrt{vb} F(\eta), \end{aligned} \tag{2.6}$$

the Eqs. (2.1) and (2.3) are identically satisfied in terms of relations Eq. (2.6). In addition, Eqs. (2.2) and (2.4) are reduced to following set of non-linear ordinary differential equations;

$$\alpha f''''(\eta) - [f'(\eta)]^2 + f''(\eta)f(\eta) + \beta f''^2(\eta)f'''(\eta) + l\beta_v[F'(\eta) - f'(\eta)] - Mf'(\eta) = 0, \quad (2.7)$$

$$F(\eta)F''(\eta) - [F'(\eta)]^2 + \beta_v[f'(\eta) - F'(\eta)] = 0. \quad (2.8)$$

Transformed boundary conditions are;

$$f'(\eta) = 1, \text{ at } \eta = 0, \\ f'(\eta) \rightarrow 0 \quad F'(\eta) \rightarrow 0, \quad F(\eta) \rightarrow f(\eta) \text{ as } \eta \rightarrow \infty, \quad (2.9)$$

where

$$\alpha = \frac{1}{\mu Ac} \beta, \quad \beta = \frac{bu_w^2}{2c^2v}, \quad l = \frac{Nm^*}{\rho}, \quad M = \frac{\sigma B_0^2}{\rho b}, \quad \tau_v = \frac{m^*}{K} \text{ and } \beta_v = \frac{1}{b\tau_v}.$$

### 3 Heat transfer analysis

The governing boundary layer heat transport equations for both fluid and dust phases are given by;

$$C_p \rho \left( u \frac{\partial T}{\partial x} + v \frac{\partial T}{\partial y} \right) = k \frac{\partial^2 T}{\partial y^2} + \frac{\rho_p c_p}{\tau_T} (T_p - T) + \frac{\rho_p}{\tau_v} (u_p - u)^2 - \frac{\partial q_r}{\partial y}, \quad (3.1)$$

$$u_p \frac{\partial T_p}{\partial x} + v_p \frac{\partial T_p}{\partial y} = -\frac{c_p}{c_m \tau_T} (T_p - T), \quad (3.2)$$

Using the Rosseland approximation for radiation, radiation heat flux is simplified as;

$$q_r = -\frac{16\sigma^*}{3k^*} T^3 \frac{dT}{dy}, \quad (3.3)$$

where  $\sigma^*$  -the Stefan-Boltzmann constant and  $k^*$  -mean absorption coefficient.  $T$  is temperature across the boundary.

In view of the Eq. (3.3), the energy Eq. (3.1) becomes;

$$C_p \rho \left( u \frac{\partial T}{\partial x} + v \frac{\partial T}{\partial y} \right) = k \left( \frac{\partial^2 T}{\partial y^2} \right) + \frac{16\sigma^*}{3k^*} \left[ T^3 \frac{\partial^2 T}{\partial y^2} + 3T^2 \left( \frac{\partial T}{\partial y} \right)^2 \right] + \frac{\rho_p c_p}{\tau_T} (T_p - T) + \frac{\rho_p}{\tau_v} (u_p - u)^2, \quad (3.4)$$

Corresponding boundary conditions for the temperature are considered as;

$$T = T_m, \quad k \left( \frac{\partial T}{\partial y} \right)_{y \rightarrow 0} = \rho [E + C_s (T_m - T_0)] v(x, 0) \text{ at } y = 0, \\ T \rightarrow T_\infty, \quad T_p \rightarrow T_\infty \text{ as } y \rightarrow \infty, \quad (3.5)$$

where  $E$  is the latent heat of the fluid, and  $C_s$  is heat capacity of the solid surface. Eq. (3.5) states that heat conducted to melting surface is equal to heat of melting plus the sensible heat required raising the solid temperature  $T_0$  to its melting temperature  $T_m$ .

$$T = T_\infty (1 + (\theta_w - 1)\theta), \quad T_p = T_\infty (1 + (\theta_w - 1)\theta_p), \quad (3.6)$$

where  $\theta_w = \frac{T_w}{T_\infty}$ ,  $\theta_w > 1$  being the temperature ratio parameter.

Using Eqs. (3.6) into (3.2) and (3.4), we obtain the following non-linear ordinary differential equations:

$$\theta''(\eta) + R \left[ (1 + (\theta_w - 1)\theta(\eta))^3 \theta''(\eta) + 3(\theta_w - 1)\theta'(\eta)(1 + (\theta_w - 1)\theta(\eta))^2 \right] + Pr \theta'(\eta)f(\eta) + lPr\beta_t (\theta_p(\eta) - \theta(\eta)) + \beta_v l EcPr [F'(\eta) - f'(\eta)]^2 = 0, \quad (3.7)$$

$$\theta'_p(\eta)F(\eta) - \gamma\beta_t [\theta_p(\eta) - \theta(\eta)] = 0, \quad (3.8)$$

with

$$Prf(0) + m\theta'(0) = 0, \quad \theta(\eta) = 0 \text{ at } \eta = 0 \\ \theta(\eta) \rightarrow 1, \quad \theta_p(\eta) \rightarrow 1 \text{ as } \eta \rightarrow \infty. \quad (3.9)$$

$$\text{where } Pr = \frac{\mu c_p}{k}, \quad R = \frac{16\sigma^* T_\infty^3}{3k^*k}, \quad Ec = \frac{u_w^2}{c_p(T_\infty - T_m)}, \quad \gamma = \frac{c_p}{c_m}, \quad \beta_t = \frac{1}{b\tau_T}.$$

$m$  -dimensionless melting parameter which is defined as  $m = \frac{c_f(T_\infty - T_m)}{\lambda + c_s(T_m - T_0)}$ , which is a combination of Stefan numbers  $\frac{c_f(T_\infty - T_m)}{\lambda}$  and  $\frac{c_s(T_m - T_0)}{\lambda}$  for liquid and solid phases, respectively.

The physical quantities of interest like skin friction coefficient ( $C_f$ ) and local Nusselt number ( $Nu_x$ ) are defined as;

$$C_f = \frac{\tau_w}{\rho u_w^2} \quad \text{and} \quad Nu_x = \frac{u_w q_w}{ak(T_\infty - T_w)}$$

where the shear stress ( $\tau_w$ ) and surface heat flux ( $q_w$ ) are given by;

$$\tau_w = \frac{A}{c} \frac{\partial u}{\partial y} + \frac{A}{2c^3} \left( \frac{\partial u}{\partial y} \right)^3 \quad \text{and} \quad q_w = -k \frac{\partial T}{\partial y} + q_r.$$

Using the non-dimensional variables, one can get;

$$\sqrt{Re_x} C_f = [\alpha f''(0) + \beta f''(0)^3] \quad \text{and} \quad \frac{1}{\sqrt{Re_x}} Nu = -[1 + R\theta_w^3] \theta'(0),$$

where  $Re_x = \frac{u_w^2}{av}$  is the local Reynold's number.

#### 4 Numerical method

The non-linear ordinary differential Eqs. (2.7)-(2.8) and (3.7)-(3.8) along with the boundary conditions Eqs. (2.9) and (3.9) are solved numerically using RKF-45 order method. In our numerical computations, the step size is chosen as  $\Delta\eta = 0.001$  and the convergence criteria were set to  $10^{-6}$ . The non-dimensional velocity and temperature profiles are shown in Figs. 2-17 for several values of different physical parameters. To validate the employed method, the authors have compared the results of  $f''(0)$  with published work. These comparisons are given in Tab. 1, and it shows that the results are in very good agreement.

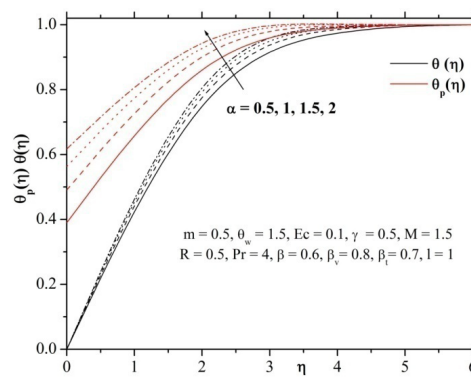
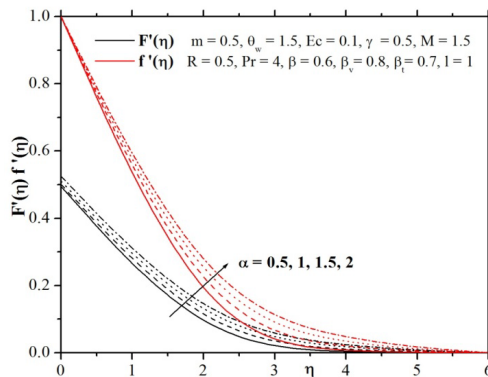
**Table 1:** Comparison values of skin friction co-efficient ( $\alpha = \beta = 0$ )

$M$	[Akbar, Nadeem, Haq et al. (2013)]	[Fathizadeh, Madani, Khan et al. (2013)]	Present result
1	-1.41421	-1.41421	-1.41421
5	-2.44948	-2.44948	-2.44949
10	-3.31662	-3.31662	-3.31662
50	-7.14142	-7.14142	-7.14143
500	-22.3830	-22.3830	-22.38302
1000	-31.6386	-31.6386	-31.63858

**5 Result and discussion**

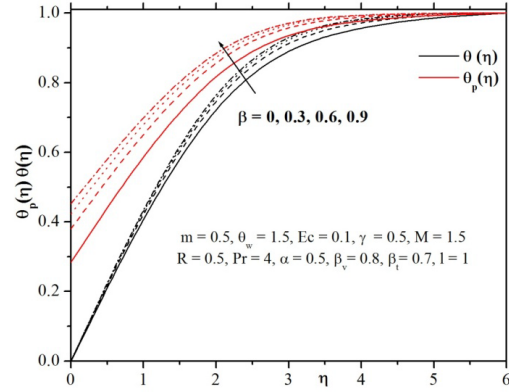
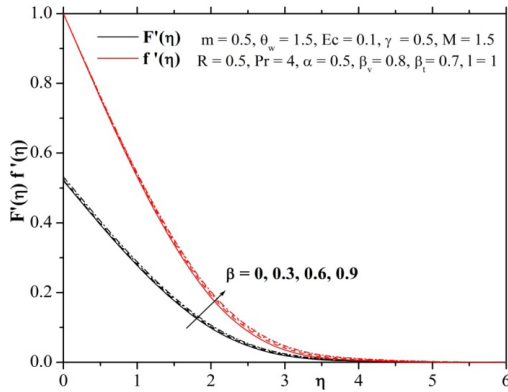
The ultimate goal of this work is to initiate the study of boundary layer flow and melting heat transfer of a Prandtl fluid over a convective surface in the presence of fluid particles suspension. In this section, we focus on the physical behaviors of the involved parameters on the velocity and temperature profiles.

Figs. 2 and 3 illustrate the variation of Prandtl parameter ( $\alpha$ ) on velocity and temperature profiles. As the value of Prandtl fluid parameter rises, the velocity of the fluid in the boundary layer increases for both phases. This is because of the increase in the Prandtl fluid parameter which results in the viscosity of fluid decrease. Consequently, fluid becomes less viscous for higher values of Prandtl fluid parameter. From Fig. 3, we observed that the dimensionless temperature profile and corresponding boundary layer thickness increases with increase in the Prandtl parameter.



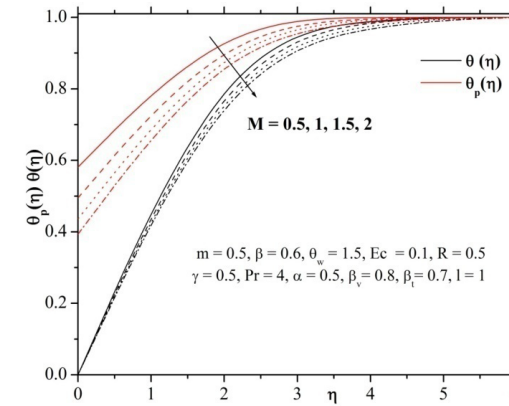
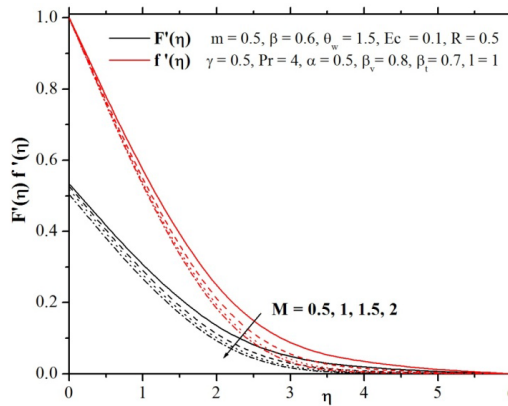
**Figure 2:** Influence of  $\alpha$  on velocity field **Figure 3:** Influence of  $\alpha$  on temperature field

Fig. 4 elaborates the curves of velocity profile for various values of elastic parameter ( $\beta$ ). It is observed that an enhancement occurred in the velocity profile and momentum boundary layer thickness when the values of elastic parameter enhance. The importance of elastic parameter on temperature profile is characterized in Fig. 5. Here, we explored that the larger values of elastic parameter enhance the temperature profile and corresponding boundary layer thickness.



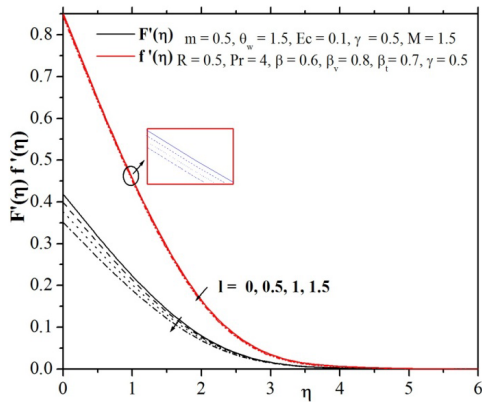
**Figure 4:** Influence of  $\beta$  on velocity field **Figure 5:** Influence of  $\beta$  on temperature field

Figs. 6 and 7 are plotted to show the variations of velocities and temperature profiles of fluid and dust phase for different values of magnetic parameter ( $M$ ). From these plots, it is observed that velocity and temperature profiles and their associated thicknesses of boundary layer reduce for the enhancement of magnetic parameter. Because resistive force tends to slow down the motion of the fluid along the plate, it causes decrease in its temperature.

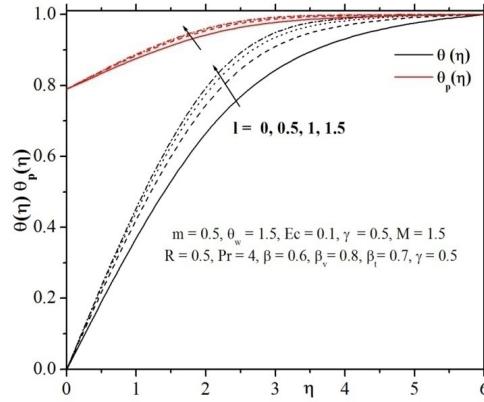


**Figure 6:** Influence of  $M$  on velocity field **Figure 7:** Influence of  $M$  on temperature field

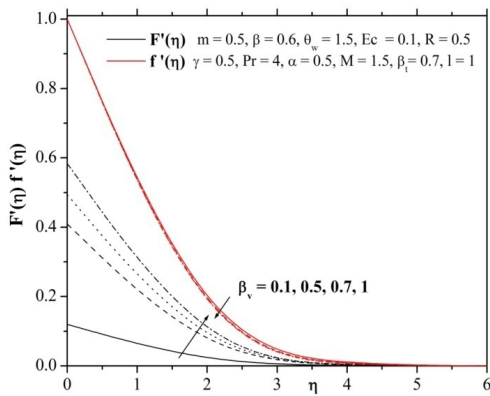
The variation of velocity and temperature profiles for both the phases are illustrated for different values of mass concentration parameter ( $l$ ), and are shown in Figs. 8 and 9 respectively. Here, the velocity profile for both the phases decreases by increasing values of mass concentration parameter and the opposite trend is observed for temperature profiles. Figs. 10 and 11 explain effect of  $\beta_v$  and  $\beta_t$  on velocity and temperature profiles, respectively. Increase of  $\beta_v$  will decrease fluid phase velocity and increase dust phase velocity. As expected, increase of  $\beta_t$  will increase fluid phase temperature, and decrease the dust phase temperature. This is because an increase in  $\beta_v$  results the decrease of  $\tau_v$ , and it is obvious that the time required by a dust particle to adjust its velocity relative to the fluid also decreases with decrease of  $\tau_v$ .



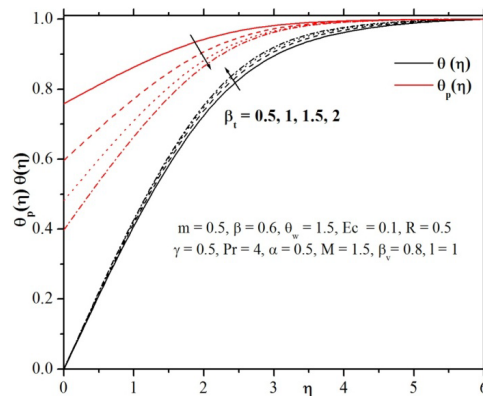
**Figure 8:** Influence of  $l$  on velocity field



**Figure 9:** Influence of  $l$  on temperature field

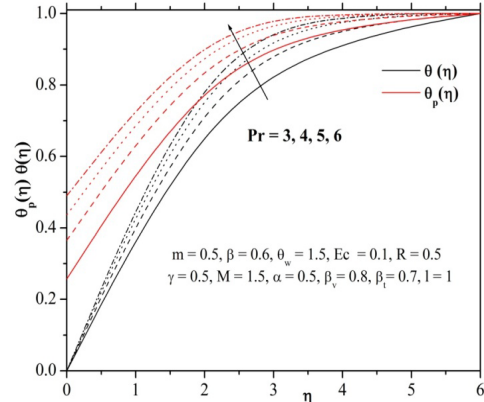
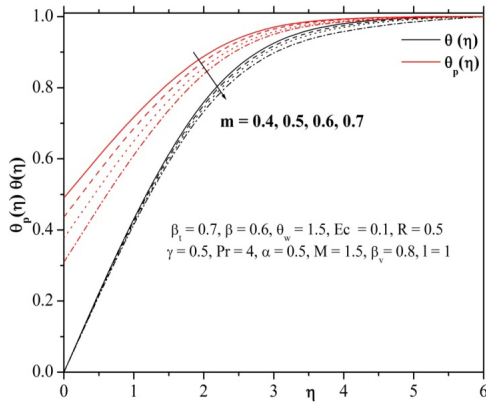


**Figure 10:** Influence of  $\beta_v$  on velocity field



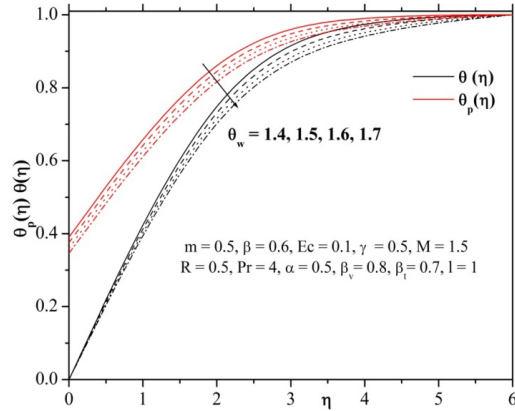
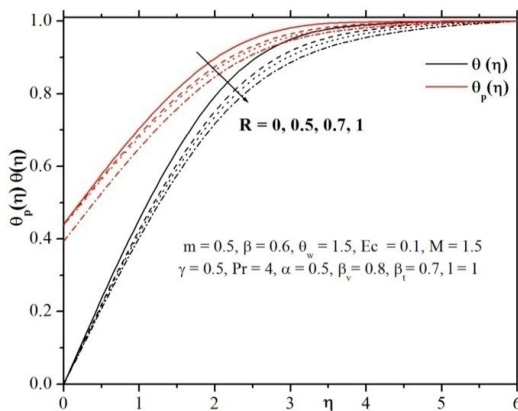
**Figure 11:** Influence of  $\beta_t$  on temperature field

Fig. 12 illustrates the influence of melting parameter ( $m$ ) on the temperature profile. An increase in the melting parameter reduces the temperature of both fluid and dust phases and also boundary layer thickness. This is because an increase in  $m$  will increase the intensity of melting as well the melting progresses. Henceforth, the sheet gradually transforms to a liquid, causing the temperature of the fluid decreases rapidly. The effect of an increase in Prandtl number on the temperature for both fluid and dust phase are captured in Fig. 13. It is obvious from this figure that the temperature and thermal boundary layer thickness increase with an increment values of  $Pr$ .



**Figure 12:** Influence of  $m$  on temperature field **Figure 13:** Influence of  $Pr$  on temperature field

The variation of temperature profile for both the phases is illustrated for different values of radiation ( $R$ ), and temperature ratio parameter ( $\theta_w$ ) are shown in Figs. 14-15. One can see that the temperature profile and thermal boundary layer thickness area unit decreased by ascent values of radiation and temperature ratio parameter. Larger values of radiation parameter manufacture a lot of heat to operating fluid that shows an associate in augmenting within temperature field. The thermal boundary thickness conjointly grows once  $R$  is exaggerated. Here, due to the effect of melting, temperature profile decreases by enhancing values of  $R$ .



**Figure 14:** Influence of  $R$  on temperature field **Figure 15:** Influence of  $\theta_w$  on temperature field

Figs. 16-17 are plotted to understand the influence of Eckert number and specific heat ratio on temperature profile. As anticipated, the temperature profile increases with increasing  $Ec$ , and this is shown in Fig. 16. From the plot 17, one can infer that thermal boundary layer thickness decreases by increasing specific heat ratio.

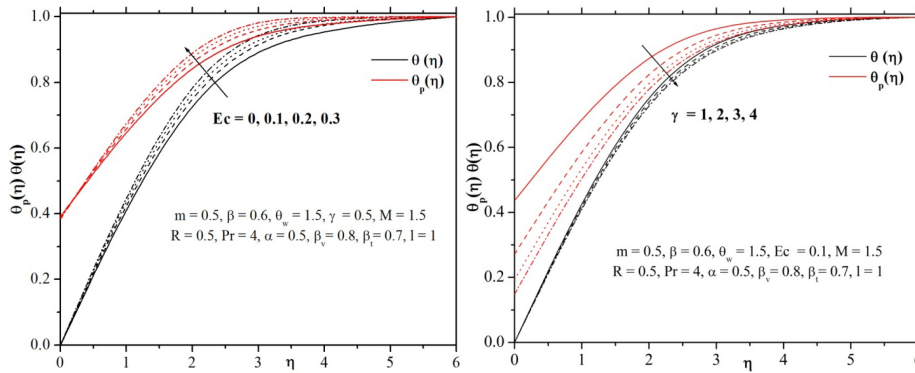


**Figure 16:** Influence of  $Ec$  on temperature field **Figure 17:** Influence of  $\gamma$  on temperature field

**Table 2:** Numerical values of skin friction coefficient and Nusselt number for different physical parameter

$\theta_w$	$Ec$	$\gamma$	$M$	$R$	$Pr$	$\alpha$	$\beta$	$\beta_v$	$\beta_t$	$l$	$m$	$-\sqrt{Re_x}C_f$	$-\frac{Nu_x}{\sqrt{Re_x}}$
1.4												2.63479	3.91105
1.5												2.63900	4.60747
1.6												2.64336	5.42572
	0.1											2.63900	4.60747
	0.2											2.64603	4.79977
	0.3											2.65276	4.98479
		1										2.62271	4.16450
		2										2.60780	3.76233
		3										2.60088	3.57642
			0.5									1.76334	5.13457
			1									2.21198	4.82621
			1.5									2.63900	4.60747
				0								2.67509	1.72441
				0.5								2.63900	4.60747
				0.7								2.62841	5.51519
					3							2.65460	3.77662
					4							2.63900	4.60747
					5							2.62754	5.36936
						0.5						2.63900	4.60747
						1						2.56062	4.98995
						1.5						2.60303	5.25357
							0					1.12917	4.16933
							0.3					2.18997	4.46087
							0.6					2.63900	4.60747
								0.1				2.38592	4.66105

	0.5	2.56616	4.60387
	0.7	2.61814	4.60373
	0.5	2.63117	4.39425
	1	2.64652	4.81342
	1.5	2.65357	5.00716
	0	2.26847	3.11317
	0.1	2.31387	3.32441
	0.3	2.35803	3.52060
	0.4	2.61249	4.86076
	0.5	2.63900	4.60747
	0.6	2.66229	4.37327

**Table 3:** Numerical values of Nusselt number for different physical parameter values for linear and nonlinear radiation

$Ec$	$\gamma$	$R$	$Pr$	$\beta_t$	$l$	$m$	$-\frac{Nu_x}{\sqrt{Re_x}}$	
							Linear radiation	Nonlinear radiation
0.1							1.24043	4.60747
0.2							1.30018	4.79977
0.3							1.35766	4.98479
	1						1.14883	4.16450
	2						1.05060	3.76233
	3						1.00014	3.57642
		0					1.50743	1.72441
		0.5					1.24043	4.60747
		0.7					1.16240	5.51519
			3				1.02387	3.77662
			4				1.24043	4.60747
			5				1.43254	5.36936
				0.5			1.17122	4.39425
				1			1.31170	4.81342
				1.5			1.38277	5.00716
					0		0.77165	3.11317
					0.1		0.83446	3.32441
					0.3		0.89188	3.52060
						0.4	1.29917	4.86076
						0.5	1.24043	4.60747
						0.6	1.18547	4.37327

Tab. 2 displays variation of skin friction coefficient and Nusselt number for different values of physical parameter. It is reported that the Nusselt number is a decreasing function of  $\gamma, \beta_v, m$  and  $M$ , but an increase can be found in increase of  $\theta_w, Ec, R, Pr, \alpha$  and  $\beta$ . Additionally, the skin friction coefficient increases while enhancing the values of

$\theta_w, Ec, M, \beta, m$  and  $\beta_v$ . Tab. 3 shows the variation of Nusselt number on different physical parameter for linear and nonlinear radiation. From this table, we observed that Nusselt numbers rates are higher in presence of nonlinear radiation compared to linear radiation.

## 6 Conclusion

The present study deals with the boundary layer flow and melting heat transfer of a Prandtl fluid over a stretching surface in the presence of nonlinear thermal radiation. The important findings of the present study are listed as follows:

- Temperature profile and rate of heat transfer is lesser for larger values of  $R$ .
- The velocity and temperature profile increases by with increasing values of  $\alpha$  and  $\beta$ .
- The temperature profile and its corresponding boundary layer is increased with increasing Prandtl number.
- Higher values of  $Ec$  enhances the thermal boundary layer thickness.
- Rate of heat transfer decreases by increasing melting parameter.
- Due to the effect of melting parameter, the rate of heat transfer decreases by increasing values of  $\theta_w$ .

**Conflict of Interest:** The authors declare that they have no conflict of interest on this research work.

## References

- Afridi, M. I.; Qasim, M.** (2018): Entropy generation and heat transfer in boundary layer flow over a thin needle moving in a parallel stream in the presence of nonlinear Rosseland radiation. *International Journal of Thermal Sciences*, vol. 123, pp. 117-128.
- Akbar, N. S.; Nadeem, S.; Haq, R. U.; Khan, Z. H.** (2013): Numerical solutions of Magneto hydrodynamic boundary layer flow of tangent hyperbolic fluid flow towards a stretching sheet with magnetic field. *Indian Journal of Physics*, vol. 87, no. 11, pp. 1121-1124.
- Arici, M.; Ensar, T.; Kan, M.; Hasan, K.** (2017): Melting of nanoparticle-enhanced paraffin wax in a rectangular enclosure with partially active walls. *International Journal of Heat and Mass Transfer*, vol. 104, pp. 7-17.
- Bachok, N.; Ishak, A.; Pop, I.** (2010): Melting heat transfer in boundary layer stagnation-point flow towards a stretching/shrinking sheet. *Physics Letters A*, vol. 374, pp. 4075-4079.
- Beg, O. A.; Thumma, T.; Kadir, A.** (2017): Numerical study of heat source/sink effects on dissipative magnetic nanofluid flow from a nonlinear incline stretching/shrinking sheet. *Journal of Molecular Liquids*, vol. 232, pp. 159-173.
- Fathizadeh, M.; Madani, M.; Khan, Y.; Faraz, N.; Yildirim A. et al.** (2013): An effective modification of the homotopy perturbation method for MHD viscous flow over a stretching sheet. *Journal of King Saud University*, vol. 25, no. 2, pp. 107-113.
- Giresha, B. J.; Kumar, K. G.; Rudraswamy, N. G.; Gorla, R. S. R.** (2017): Melting heat transfer of hyperbolic tangent fluid over a stretching sheet with fluid particle suspension and thermal radiation. *Communications in Numerical Analysis*, vol. 2, no. 2017, pp. 125-140.

- Gireesha, B. J.; Ramesh, G. K.; Kumar, K. G.; Prasannakumar, B. C.** (2018): Nonlinear convective heat and mass transfer of Oldroyd-B nanofluid over a stretching sheet in the presence of uniform heat source/sink. *Results in Physics*, vol. 9, pp. 1555-1563.
- Hayat, T.; Qayyum, S.; Imtiaz, M.; Alsaedi, A.** (2016): Comparative study of silver and copper water nanofluids with mixed convection and nonlinear thermal radiation. *International Journal of Heat and Mass Transfer*, vol. 102, pp. 723-732.
- Hussain, A.; Malik, M. Y.; Awais, M.; Salahuddin, T.; Bilal, S.** (2017): Computational and physical aspects of MHD Prandtl-Eyring fluid flow analysis over a stretching sheet. *Neural Computation and Application*.
- Isa, S. M.; Mohammad, N. F.** (2017): Boundary layer flow of dusty fluid on a stretching sheet of another quiescent fluid. *Journal of Physics: Conference Series*, vol. 819, no. 1, 012027.
- Khan, I.; Malik, M. Y.; Hussain, A.; Salahuddin, T.** (2017): Effect of homogenous-heterogeneous reactions on MHD Prandtl fluid flow over a stretching sheet. *Results in Physics*, vol. 7, pp. 4226-4231.
- Krishnamurthy, M. R.; Kumar, K. G.; Gireesha, B. J.; Rudraswamy, N. G.** (2018): MHD flow and heat transfer (PST and PHF) of dusty fluid suspended with alumina nanoparticles over a stretching sheet. *Journal of Nanofluids*, vol. 7, no. 3, pp. 527-535.
- Kumar, K. G.; Archana, M.; Gireesha, B. J.; Krishnamurthy, M. R.; Rudraswamy, N. G.** (2018): Cross diffusion effect on MHD mixed convection flow of nonlinear radiative heat and mass transfer of Casson fluid over a vertical plate. *Results in Physics*, vol. 8, pp. 694-701.
- Kumar, K. G.; Gireesha, B. J.; Gorla, R. S. R.** (2018): Flow and heat transfer of dusty hyperbolic tangent fluid over a stretching sheet in the presence of thermal radiation and magnetic field. *International Journal of Mechanical and Materials Engineering*, vol. 13, no. 1, pp. 2.
- Kumar, K. G.; Gireesha, B. J.; Prasannakumara, B. C.; Ramesh, G. K.** (2017): Phenomenon of radiation and viscous dissipation on Casson nanoliquid flow past a moving melting surface. *Diffusion Foundations*, vol. 11, pp. 33-42.
- Kumar, K. G.; Manjunatha, S.; Gireesha, B. J.; Rudraswamy, N. G.** (2017): Radiative heat transfers of Carreau fluid flow over a stretching sheet with fluid particle suspension and temperature jump. *Results in Physics*, vol. 7, pp. 3976-3983.
- Kumar, K. G.; Rudraswamy, N. G.; Gireesha, B. J.; Manjunatha, S.** (2017): Nonlinear thermal radiation effect on Williamson fluid with particle-liquid suspension past a stretching surface. *Results in Physics*, vol. 7, pp. 3196-3202.
- Mabood, F.; Shafiq, A.; Hayat, T.; Abelman, S.** (2017): Radiation effects on stagnation point flow with melting heat transfer and second order slip. *Results in Physics*, vol. 7, pp. 31-42.
- Makinde, O. D.; Kumar, K. G.; Manjunatha, S.; Gireesha, B. J.** (2017): Effect of nonlinear thermal radiation on MHD boundary layer flow and melting heat transfer of micro-polar fluid over a stretching surface. *Defect and Diffusion Forum*, vol. 378, pp. 125-136.

**Makinde, O. D.; Animasaun, I. L.** (2016): Thermophoresis and brownian motion effects on MHD bioconvection of nanofluid with nonlinear thermal radiation and quartic chemical reaction past an upper horizontal surface of a paraboloid of revolution. *Journal of Molecular Liquids*, vol. 221, pp. 733-743.

**Malik, M. Y.; Hussain, A.; Salahuddin, T.; Awais, M.** (2016): Numerical solution of MHD Sisko fluid over a stretching cylinder and heat transfer analysis. *International Journal of Numerical Methods for Heat & Fluid Flow*, vol. 26, no. 6, pp. 1787-1801.

**Mishra, S. R.; Khan, I.; Al-mdallal, Q. M.; Asifa, T.** (2015): Free convective micropolar fluid flow and heat transfer over a shrinking sheet with heat source. *Alexandria Engineering Journal*, vol. 54, no. 3, pp. 681-689.

**Mohsen, S.; Sadoughi, M. K.** (2018): Simulation of CuO-water nanofluid heat transfer enhancement in presence of melting surface. *International Journal of Heat and Mass Transfer*, vol. 116, pp. 909-919.

**Mustafa, T.** (2017): Magnetohydrodynamic two-phase dusty fluid flow and heat model over deforming isothermal surfaces. *Physics of Fluids*, vol. 29, 013302.

**Nasrin, R.; Alim, M. A.** (2012): Prandtl number effect on free convective flow in a solar collector utilizing nanofluid. *Engineering e-Transaction*, vol. 7, no. 2, pp. 62-72.

**Prakash, O. M.; Makinde, O. D.; Kumar, D.; Dwivedi, Y. K.** (2015): Heat transfer to MHD oscillatory dusty fluid flow in a channel filled with a porous medium. *Sadhan*, vol. 40, no. 4, pp. 1273-1282.

**Reddy, M. G.; Rani, M. S.; Kumar, K. G.; Prasannakumara, B. C.** (2018): Cattaneo-Christov heat flux and non-uniform heat-source/sink impacts on radiative Oldroyd-B two-phase flow across a cone/wedge. *Journal of the Brazilian Society of Mechanical Sciences and Engineering*, vol. 40, no. 2, pp. 95.

**Nasrin, R.; Parvin, S.; Alim, M. A.** (2016): Prandtl number effect on assisted convective heat transfer through a solar collector. *Applications and Applied Mathematics: An International Journal*, vol. 2, pp. 22-36.

**Saffman, P. G.** (1962): On the stability of laminar flow of a dusty gas. *Journal of Fluid Mechanics*, vol. 13, pp. 120-128.

**Shamshuddin, M. D.; Beg, O. A.; Ram, M. S.; Kadir, A.** (2017): Finite element computation of multi-physical Micropolar transport phenomena from an inclined moving plate in porous media. *Indian Journal of Physics*, vol. 92, no. 2, pp. 215-230.

**Siddiqa, S.; Hossain, M. A.; Saha, S. C.** (2015): Two-phase natural convection flow of a dusty fluid. *International Journal of Numerical Methods for Heat & Fluid Flow*, vol. 25, no. 7, pp. 1542-1556.

**Nadeem, S.; Ijaz, S.; Akbar, N. S.** (2013): Nanoparticle analysis for blood flow of Prandtl fluid model with stenosis. *International Journal of Nano Letters*, vol. 3, no. 35, pp. 2-13.

**Thumma, T.; Shamshuddin, M. D.** (2018): Buoyancy ratio and heat source effects on MHD flow over an inclined non-linearly stretching sheet. *Frontiers in Heat and Mass Transfer*, vol. 10, pp. 1-12.